# *Ab Initio* Study on the Unimolecular Decomposition Mechanisms and Spectroscopic Properties of $CH_3OF$

**Yitzhak Apeloig* and Karsten Albrecht**

*Contribution from the Department of Chemistry, Technion-Israel Institute of Technology, Technion City, 32000 Haifa, Israel*

*Received March 27, 1995*[⊗]

**Abstract:** High-level *ab initio* calculations of the structure, vibrational frequencies, and NMR spectra of the recently isolated methyl hypofluorite, $CH_3OF$, have been carried out. When electron correlation is included in the calculations (but not at the HF level), there is a very good agreement between the experimental and the theoretical IR and NMR spectra. Four different unimolecular decomposition pathways, all leading to $CH_2O$ and HF, were studied. Of these, two mechanisms, the synchronous single-step HF elimination and a two-step mechanism *via* the $CH_3O^•$ and $F^•$ radicals, are predicted to be the most favorable, both having activation free energies of ca. 38 kcal $mol^{-1}$ at GAUSSIAN 2. A theoretical analysis of the expected kinetic isotope effects between the competing pathways leads to a clear differentiation which can be used in experimental studies.

## Introduction

Hypofluorites (ROF) are usually kinetically unstable compounds, and the only molecules of this type that persist for a long time at ambient temperatures are ones in which the O−F unit is bonded either directly to another fluorine atom ($OF_2$) or indirectly to a perfluorinated moiety ($CF_3OF$, $F_5SOF$).[1] However, more recently hypofluorous acid, HOF,[2] and acetyl hypofluorite, $CH_3C(O)OF$,[3] have been synthesized and characterized spectroscopically. In 1991, Rozen and co-workers reported the isolation and characterization by IR, NMR, and mass spectroscopy of the first alkyl hypofluorite, $CH_3OF$,[4] and showed that it can be used effectively in synthesis as a synthon of the previously unknown electrophilic methylium cation ("$CH_3O^+$").[5] Subsequently in 1993, the synthesis and characterization of *tert*-butyl hypofluorite, $(H_3C)_3COF$, was also reported.[6]

$CH_3OF$ not only is a novel and versatile synthetic reagent but also raises many interesting fundamental questions regarding its kinetic and thermodynamic stability, its structure, and its spectroscopic properties. Molecules having bonds between highly electronegative atoms, as in $CH_3OF$, present also a computational challenge, and it is of interest to determine which theoretical level can reproduce their physical and chemical properties. In this paper we report extensive calculations for $CH_3OF$ using reliable post-Hartree−Fock *ab initio* methods, including computations of its IR and NMR spectra and a detailed study of possible pathways for its unimolecular decomposition.

## Computational Methods

*Ab initio* molecular orbital calculations[7] were performed using the GAUSSIAN 92 series of programs.[8] Equilibrium geometries and transition structures were fully optimized using gradient techniques, and vibrational frequencies were computed for all species, in order to characterize them as minima, transition structures, or higher order saddle points on the potential energy surface (PES) and for evaluating their zero-point energies. The standard 6-31G*,[9] 6-311G*,[10] and 6-311+G**[11] basis sets were employed. The effect of correlation energy was included by using the Møller−Plesset perturbation theory up to fourth order (MP4), with either frozen core (fc) or full (fu) electron correlation which includes also the inner-shell electrons. The GAUSSIAN 2 (G2)[12] procedure which is based on MP4 energies with the 6-311G** basis set, modified by a series of additive corrections to approximate a QCISD(T)/6-311+G(3df,2p) calculation, was used to obtain reliable relative energies of the investigated species. Deuterium and $^{13}C$ isotope effects were calculated with the QUIVER program[13] using the calculated MP2(fu)/6-31G* force constants. The calculated harmonic frequencies were corrected by a factor of 0.9427[14] for the MP2/6-31G*, MP2/6-311G*, and MP2/6-311+G** computations and by a factor of 0.8929[14] for the RHF/6-31G* and RHF/6-311G* calculations.[15] NMR chemical shieldings were calculated employing the IGLO[16] and the GIAO[17]

⊗ Abstract published in *Advance ACS Abstracts*, August 1, 1995.

(1) Prager, J. H.; Thompson, P. G. *J. Am. Chem. Soc.* **1965**, *87*, 230.
(2) Studier, M. H.; Appelman, E. H. *J. Am. Chem. Soc.* **1971**, *93*, 2349.
(3) (a) Rozen, S.; Lerman, O.; Kol, M. *J. Chem. Soc., Chem. Commun.* **1981**, 443. (b) Appelman, E. H.; Mendelsohn, M. H.; Kim, H. *J. Am. Chem. Soc.* **1985**, *107*, 6515.
(4) Kol, M.; Rozen, S.; Appelman, E. *J. Am. Chem. Soc.* **1991**, *113*, 2648.
(5) (a) Rozen, S.; Mishani, E.; Kol, M. *J. Am. Chem. Soc.* **1992**, *114*, 7643. (b) Kol, M.; Rozen, S. *J. Org. Chem.* **1993**, *58*, 1593. (c) McCarthy, T. J.; Bonasera, T. A.; Welch, M. J.; Rozen, S. *J. Chem. Soc., Chem. Commun.* **1993**, 561.
(6) Appelman, E. H.; French, D.; Mishani, E.; Rozen, S. *J. Am. Chem. Soc.* **1993**, *115*, 1379.
(7) Hehre, W. J.; Radom, L.; Schleyer, P. v. R.; Pople, J. A. *Ab Initio Molecular Orbital Theory*; John Wiley & Sons: New York, 1986.
(8) Frisch, M. J.; Trucks, G. W.; Head-Gordon, M.; Gill, P. M. W.; Wong, M. W.; Foresman, J. B.; Johnson, B. G.; Schlegel, H. B.; Robb, M. A.; Replogle, E. S.; Goperts, R.; Andres, J. L.; Raghavachari, K.; Binkley, J. S.; Gonzalez, C.; Martin, R. L.; Fox, D. J.; DeFrees, D. J.; Baker, J.; Stewart, J. J. P.; Pople, J. A. *GAUSSIAN 92*, Revision C; Gaussian Inc.: Pittsburgh, 1992.
(9) Gordon, M. S.; Binkley, J. S.; Pople, J. A.; Pietro, W. J.; Hehre, W. J. *J. Am. Chem. Soc.* **1982**, *104*, 2797.
(10) Binkley, J. S.; Pople, J. A.; Hehre, W. J. *J. Am. Chem. Soc.* **1980**, *102*, 939.
(11) Pietro, W. J.; Francl, M. M.; Hehre, W. J.; DeFrees, D. J.; Pople, J. A.; Binkley, J. S. *J. Am. Chem. Soc.* **1982**, *104*, 5039.
(12) (a) Pople, J. A.; Head-Gordon, M.; Fox, D. J.; Raghavachari, K.; Curtiss, L. A. *J. Chem. Phys.* **1989**, *90*, 5622. (b) Curtiss, L. A.; Raghacachari, K.; Trucks, G. W.; Pople, J. A. *J. Chem. Phys.* **1991**, *94*, 7221.
(13) Saunders, M.; Laidig, K. E.; Wolfsberg, M. *J. Am. Chem. Soc.* **1989**, *111*, 8989.
(14) These empirical correction factors were designed for the 6-31G* basis set, and they do not necessarily apply to the larger 6-311G* and 6-311+G** basis sets, where the correction factors are expected to be closer to 1.[15]
(15) Pople, J. A.; Scott, A. P.; Wong, W.; Radom, L. *Isr. J. Chem.* **1993**, *33*, 345.
(16) Schindler, M.; Kutzelnigg, W. *J. Chem. Phys.* **1982**, *76*, 1919.
(17) Gauss, J. *Chem. Phys. Lett.* **1992**, *191*, 614.

0002-7863/95/1517-9564$09.00/0 

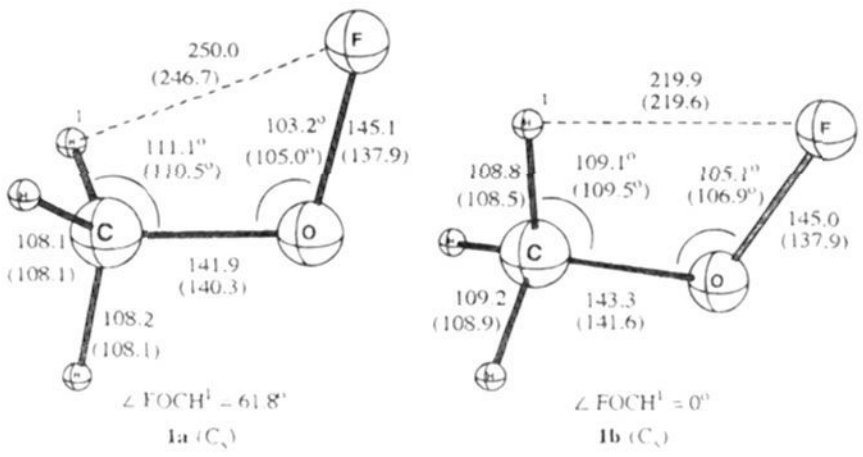


**Figure 1.** Optimized structures of the staggered (**1a**) and eclipsed (**1b**) conformations of $CH_3OF$ at MP2(fu)/6-31G* (values in parentheses are at RHF/6-31G*). Distances in picometers, angles in degrees.

(incorporated in the ACES II program[18]) methods, the latter method allowing the inclusion of electron correlation.

## Results and Discussion

**1. Equilibrium Geometries.** The equilibrium geometry of $CH_3OF$ (**1**) was calculated at the Hartree−Fock level (HF) as well as with the second-order Møller−Plesset perturbation theory (MP2), using the standard 6-31G* and 6-311+G** basis sets. The only minimum on the PES is the staggered conformer **1a**, and its optimized geometry, as well as that of the eclipsed conformer **1b** (a saddle point), is shown in Figure 1. In general,

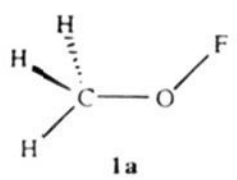


**1a**

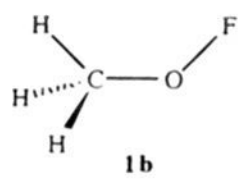


**1b**

the geometries of **1a** and **1b** are very similar. The calculated bond lengths are somewhat longer at the MP2 level than at HF, particularly for the C−O and O−F distances, which for **1a** are C−O = 140.3 pm and O−F = 137.9 pm at RHF/6-31G* and C−O = 141.9 pm and O−F = 145.1 pm at MP2(fu)/6-31G*. The C−O bond length in **1a** of 141.9 pm is similar to that in $H_3COH$ (141.3 pm). The O−F bond length in HOF of 144.5 pm (at MP2(fu)/6-31G*) is almost the same as in **1a**, showing that the methyl effect is small (for HOF, the O−F bond length is 7.0 pm longer at MP2(fu)/6-31G* than at RHF/6-31G*). The FOC bond angle in **1a** is 103.2°, significantly wider than the 97.1° bond angle in HOF, probably reflecting some steric interactions in **1a**. **1b** is the transition structure for rotation around the C−O bond, lying 4 kcal $mol^{-1}$ higher in energy at MP4/6-311+G**//MP2(fu)/6-31G* than **1a**. The relatively high barrier for rotation around the C−O bond, 3 kcal $mol^{-1}$ higher than in methanol, can be explained by larger stabilizing $\sigma$-hyperconjugative and $\pi$-type conjugative interactions in **1a** relative to those in **1b**.[19]

**2. IR Spectra.** The IR frequencies of **1** were calculated at various levels of theory, and the results are presented and compared with the experimental data in Table 1. The calculated vibration frequencies usually decrease when larger basis sets are used and when electron correlation is included in the calculations. In particular, the vibrations arising from the O−F bond differ by as much as 80 $cm^{-1}$ between the HF and the MP2 calculations.

Comparison between the HF calculated vibrations and the experimental data shows only poor agreement. However, the calculated frequencies using the MP2 theory with triple-$\zeta$ basis sets (corrected by a factor of 0.9427[14,15]) give very good agreement with experiment, the largest deviation between the calculated and the measured vibrational frequencies being less than 15 $cm^{-1}$, with the average difference being only 9 $cm^{-1}$. In agreement with previous literature assignments for the IR spectra of **1**[4] and $CF_3OF$,[20] we also find that the vibrational frequencies between 2991 and 1188 $cm^{-1}$ are due, according to calculations, to C−H stretching (2991 and 2914 $cm^{-1}$), C−H deformation (1479, 1467, and 1406 $cm^{-1}$), and C−H rock vibrations (1188 $cm^{-1}$). Furthermore, the computational data allow the measured IR frequencies at 824 and 994 $cm^{-1}$ to be assigned with confidence to O−F stretching and to a complex O−F and C−O stretching vibration mode, respectively. The assignment of these bands from the experiment was ambiguous.[4]

**3. NMR Spectra.** The NMR chemical shifts of $CH_3OF$ were reported to be 70.3 ppm for $^{13}C$ and 120.0 ppm for $^{19}F$ ($CFCl_3$ was used as the external standard).[4] The $^{19}F$ chemical shift in **1** is strongly deshielded relative to that in HOF (21 ppm),[21] but it is more shielded than in $CF_3OF$ (147 ppm), $C_2F_5OF$ (139 ppm),[22] and $H_3CC(=O)OF$ (168 ppm).[23]

*Satisfactory agreement between calculated and measured* $^{19}F$ chemical shifts has been demonstrated for a variety of compounds by using the IGLO (individual gauge for localized orbitals) method developed by Kutzelnigg and Schindler,[16] but in some cases where electron correlation plays an important role the theoretical−experimental agreement is poor.[24] Recently, a correlated method for calculating NMR chemical shifts based on the GIAO (gauge-including atomic orbitals) method at the second-order many-body perturbation theory (MBPT(2)) was developed,[17] and for several nuclei excellent theoretical−experimental agreement was achieved.[25] We have calculated the NMR chemical shifts for $CH_3OF$ (MP2(fu)/6-31G* geometry) using both the IGLO (basis II) and the GIAO (basis tzp and qzp)[26] methods. The calculated data are presented in Table 2.

With both methods the calculated $^{13}C$ NMR resonances for $CH_3OF$ are in the range of 62−68 ppm, in reasonably good agreement with the experimental value of 70.3 ppm. The smallest deviation from experiment of only 2.1 ppm is obtained with the GIAO−MBPT(2) method using the largest qzp basis set. For the $^{13}C$ chemical shift of $CH_3OF$ the addition of electron correlation is of only moderate importance; the IGLO calculated chemical shift is 7.8 ppm from the experimental value. The situation is dramatically different for the fluorine chemical shift where at the SCF level both the IGLO and the GIAO−SCF methods fail to reproduce, even qualitatively, the experimental data, predicting shifts which deviate from experiment by as much as 100 and 120 ppm upfield. However, when electron correlation is included in the calculations, the GIAO−MBPT(2) values are in fairly good agreement with experiment, and the results improve even further using a large basis set such as qzp, where the deviation from the experimental value is only 12.7 ppm (Table 2). Thus, electron correlation plays a major

(18) Stanton, J. F.; Gauss, J.; Watts, J. D.; Lauderdale, W. J.; Bartlett, R. J. *Int. J. Quantum Chem., Quantum Chem. Symp.* **1992**, *26*, 879.

(19) For a recent study on the internal rotational barriers in derivatives of methanol, see: Wu, Y.-D.; Houk, K. N. *J. Phys. Chem.* **1990**, *94*, 4856.

(20) (a) M. Falk, M.; E. Whalley, E. *J. Chem. Phys.* **1961**, *34*, 1554. (b) Wilt, P. M.; Jones, E. A. *J. Inorg. Nucl. Chem.* **1968**, *30*, 2933.

(21) Hindman, J. C.; Svirmickas, A.; Appelman, E. H. *J. Chem. Phys.* **1972**, *57*, 4542.

(22) Lustig, M.; Shreeve, J. M. In *Advances in Fluorine Chemistry*; Tatlow, J. C., Peacock, R. D., Hyman, H. H., Eds.; Butterworth: London, 1973; Vol. 7, p 175.

(23) Appelman, E. H.; Mendelsohn, M. H.; Kim, H. J. *J. Am. Chem. Soc.* **1985**, *107*, 6515.

(24) (a) Fleischer, U.; Schindler, M. *Chem. Phys.* **1988**, *120*, 103. (b) For a review see: Kutzelnigg, W.; Fleischer, U.; Schindler, M. *NMR: Basic Princ. Prog.* **1990**, *20*, 173.

(25) Gauss, J. *J. Chem. Phys.* **1993**, *99*, 3629.

(26) Schaefer, A.; Horn, H.; Ahlrichs, R. *J. Chem. Phys.* **1992**, *97*, 2571.

**Table 1.** Calculated (**1a**) and Experimental Vibrational Frequencies[a] of $CH_3OF$ ($cm^{-1}$)

| RHF/6-31G*[b] | RHF/6-311+G**[b] | MP2(fc)/6-31G*[c] | MP2(fu)/6-31G*[c] | MP2(fc)/6-311G*[c] | MP2(fc)/6-311+G**[c] | exptl[4,a] | assignment[d] |
|---|---|---|---|---|---|---|---|
| 922 | 912 | 861 | 862(10)[e] | 835 | 815(12)[e] | 824(s) | OF stretch |
| 1090 | 1079 | 1001 | 1004(13) | 999 | 983(15) | 994(m) | OF/CO stretch |
| 1154 | 1140 | 1137 | 1139(1) | 1141 | 1127(1) | | CH rock |
| 1205 | 1194 | 1170 | 1172(3) | 1176 | 1160(5) | 1188(m) | CH rock |
| 1433 | 1410 | 1411 | 1413(1) | 1406 | 1386(1) | | CH def |
| 1445 | 1416 | 1434 | 1435(6) | 1414 | 1390(8) | 1418(m) | CH def |
| | | | | | | 1467(m) | CH def |
| 1483 | 1458 | 1485 | 1487(8) | 1470 | 1451(10) | 1479(m) | CH def |
| 2891 | 2849 | 2931 | 2932(15) | 2906 | 2901(17) | 2914(m) | CH stretch |
| 2970 | 2926 | 3029 | 3030(26) | 3003 | 3003(23) | 2991(s) | CH stretch |
| 2975 | 2936 | 3037 | 3039(9) | 3015 | 3007(8) | | CH stretch |

[a] Values in parentheses denote the calculated relative intensities (s = strong, m = medium). [b] Corrected by a factor of 0.8929. [c] Corrected by a factor of 0.9427. [d] According to the calculations. [e] Values in parenteses denote the calculated relative intensities.

**Table 2.** Calculated and Measured $^{19}F$ and $^{13}C$ NMR Chemical Shifts of $CH_3OF$ (**1a**)[a]

| basis | IGLO basis II | GIAO–SCF tzp | GIAO–SCF qzp/tzp[b] | GIAO–MBPT(2) tzp | GIAO–MBPT(2) qzp/tzp[b] | exptl |
|---|---|---|---|---|---|---|
| $^{13}C$ | 62.5 | 67.2 | 68.2 | 67.2 | 68.2 | 70.3 |
| $^{19}F$ | 22.3 | 37.9 | 26.7 | 149.5 | 132.7 | 120.0 |

[a] All values are given with respect to TMS (for $^{13}C$) and $CFCl_3$ (for $^{19}F$). [b] qzp for O and F, tzp for C and H.

role in properly describing the fluorine chemical shift in $CH_3OF$. Similar conclusions are reached for the $^{19}F$ chemical shifts in HOF, which are calculated to be −28.4 ppm (tzp) and −43.1 ppm (qzp) at the SCF level of theory and 53.7 ppm (tzp) and 33.6 ppm (qzp) using the GIAO–MBPT(2) method, compared to the experimental value of 21 ppm.[21] The best agreement between the measured and the calculated values for the $^{19}F$ chemical shift in HOF is found at the GIAO–MBPT(2)/qzp//MP2(fu)/6-31G* level of theory with a deviation of only 12 ppm (in comparison with a deviation of more than 50 ppm at the SCF/tzp//MP2(fu)/6-31G* level).

**4. Unimolecular Decomposition Pathways.** The successful isolation and the relatively high kinetic stability of $CH_3OF$ (**1**) were unexpected because it was generally believed that alkyl hypofluorites having α-hydrogens will easily eliminate HF with concomitant formation of a C=O double bond (eq 1).[3-5] $CH_3OF$ indeed decomposes according to eq 1, but at much higher temperatures than was originally anticipated. Despite the considerable synthetic interest in $CH_3OF$, nothing is known on the thermodynamics or the kinetics of its decomposition reaction either in the gas phase or in solution. There is also considerable interest in this issue from a mechanistic aspect. We have therefore computationally studied in detail the possible unimolecular decomposition mechanisms of $CH_3OF$ in the gas phase, hoping to provide a better understanding of the factors which control its lifetime. We did not consider in this study bimolecular processes, which might occur in solution.

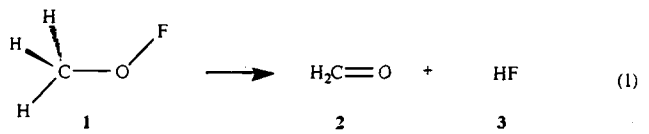


Four unimolecular decomposition pathways of **1**, shown in Scheme 1, all leading to HF and $H_2C=O$, were characterized computationally as genuine reaction mechanisms by using the intrinsic reaction coordinates (IRC) method for following the reaction path. The first unimolecular decomposition pathway involves HF elimination in a single step (path *a* in Scheme 1), and the three other involve stepwise mechanisms (paths *b*–*d* in Scheme 1). What follows is a detailed discussion of these decomposition pathways of **1**.

**Scheme 1.** Mechanisms for the Unimolecular Decomposition of **1** to $H_2C=O$ + HF

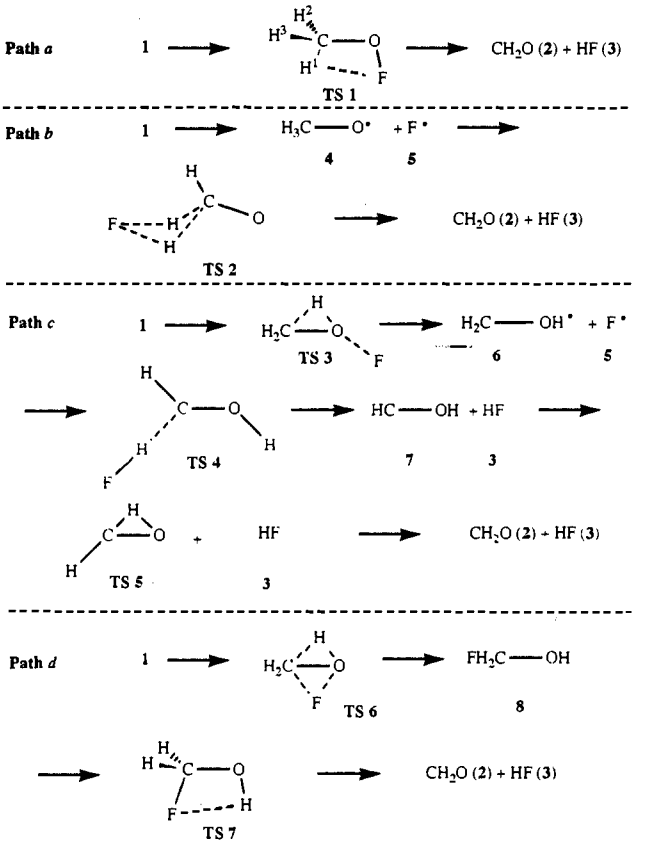


**a. Transition State Geometries.** The calculated geometries at MP2(fu)/6-31G* of the various transition states which were characterized along the four decomposition pathways shown in Scheme 1 are given in Figure 2. The transition state for the synchronous single-step HF elimination (**TS 1**) has a distorted four-centered structure. In general **TS 1** can be described as occurring "late" along the reaction path. The C—H and O—F bonds in **TS 1** are significantly elongated compared to the ground state of **1**, i.e., to 145.4 pm (by ca. 40%) for C—H and to 179.7 pm (by ca. 35%) for the O—F bond. The C—O bond length is shortened substantially from 143.3 pm in **1b** to 106.2 pm in **TS 1**, becoming even shorter than the C=O length in $H_2C=O$ (118.0 ppm). The H—F distance in **TS 1** of 144.1 pm is ca. 50% longer than in HF (92.6 pm), but it is substantially shorter than the intermolecular H···F distance in the HF dimer (185.6 pm) or in **1b** (219.9 pm).

Decomposition pathway *b* involves an initial cleavage of the O—F bond, yielding the $CH_3O^•$ (**4**) and $F^•$ (**5**) radicals (no TS was located along this step), followed by attack of the fluorine

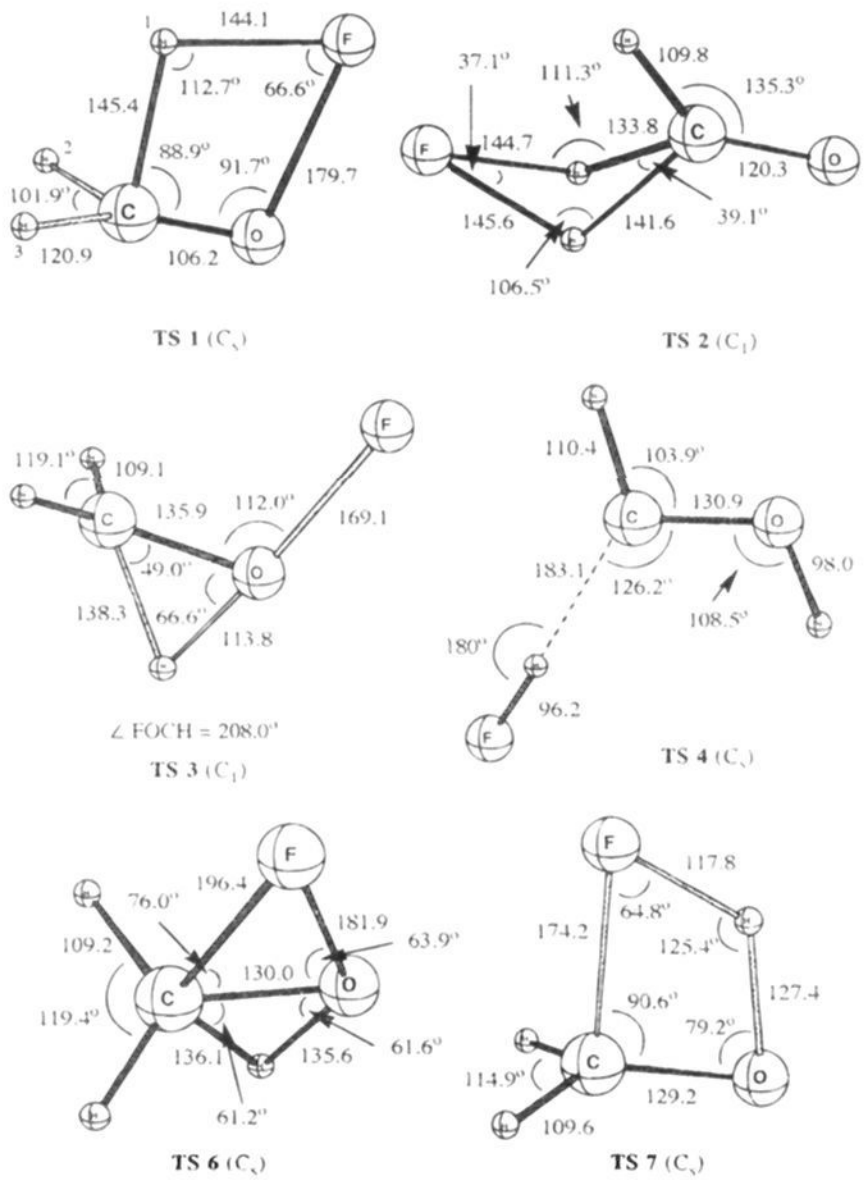


**Figure 2.** Transition structures for the decomposition of **1** at MP2-(fu)/6-31G*. Distances in picometers, angles in degrees.

atom simultaneously at two C−H bonds, leading *via* **TS 2** to HF and formaldehyde.[27] Transition structure **TS 2** has $C_1$ symmetry with two very similar F···H distances of 145.6 and 144.7 pm and two strongly elongated C−H bonds (133.8 and 141.6 pm); the C−H bond which is not directly involved in the reaction remains almost unchanged from that in **1**.

Reaction pathway *c* involves in the first step decomposition of **1** to the $CH_2OH^\bullet$ (**6**) and $F^\bullet$ radicals, which involves a simultaneous O−F bond cleavage and a 1,2 hydrogen shift *via* **TS 3**. In **TS 3** the O−F bond is substantially elongated to 169.1 pm (144.1 pm in **1a**), and the hydrogen has almost completely migrated to the oxygen (*O−H = 113.8 pm, C−H = 138.3 pm*), with HOC and HCO bond angles of 66.6° and 49.0°, respectively. Thus, **TS 3** can be described as late. The next step along mechanism *c* involves hydrogen abstraction by the fluorine atom, either from carbon or from the OH group. As the O−H bond dissociation energy is 20 kcal $mol^{-1}$ larger than the C−H bond dissociation energy,[28] the lowest transition state connecting $CH_2OH^\bullet/F^\bullet$ with $CH_2O/HF$ involves a fluorine atom attack at one of the C−H bonds of $H_2COH$.[27] The corresponding transition state, **TS 4**, can be described as a loose complex between hydroxycarbene (**7**) and HF. The final step along mechanism *c* is a rearrangement of the carbene **7** to formaldehyde *via* **TS 5**, a process which has been studied previously[29] using lower levels of theory. The migrating hydrogen in **TS 5** ($C_s$ symmetry) on the way to formaldehyde is located almost at the same distance between the oxygen and the carbon (H···O = 115.9 pm, C···H = 127.5 pm), but the C−O bond distance of 132.2 pm in **TS 5** is not shortened compared to that in HCOH.

Pathway *d* involves a simultaneous diatropic migration of hydrogen and fluorine *via* **TS 6** to give fluoromethanol (**8**).[30] In **TS 6** the two migrating hydrogens and fluorine are located roughly at the same distance from the migration termini (F−C = 196.4 pm, F−O = 181.9 pm, H−C = 136.1 pm, H−O = 135.6 pm). The C−O bond length in **TS 6** of 130.0 pm is significantly shorter than the calculated bond length in **1a** (141.9 pm) or in **8** (138.5 pm). Pathway *d* is completed by elimination of HF from $FCH_2OH$ *via* the four-centered **TS 7**, a process which has been studied earlier.[31,32] At MP2(fu)/6-31G*, the C−O bond in **TS 7** is slightly shortened to 129.2 pm from 138.5 pm in **8** and the C−F and O−H bonds are significantly elongated to 174.2 and 127.4 pm compared to 138.5 and 97.3 pm in **8**. The H···F distance in **TS 7** of 117.8 pm is ca. 30% longer than that in HF and much shorter than in the isomeric **TS 1** (144.1 pm).

**b. Energetics.** The total and relative energies for the minima and the saddle points (transition states) located along the reaction paths of Scheme 1 using the MP4/6-311+G**, G1, and G2 levels of theory (all at MP2(fu)/6-31G* optimized geometries) are presented in Table 3. The most important results are also displayed graphically in Chart 1.

It was demonstrated previously that relative energies calculated at the G1 and G2 levels of theory usually agree well with experimental data.[12] In general we find that the calculated activation barriers ($\Delta E$) are similar using either the G1 or the G2 methology, with a maximum deviation of 2.4 kcal $mol^{-1}$ between the two methods. The following discussion will be based on the G2 results which are believed to be more reliable.[12]

The decomposition reaction of **1** to $CH_2O$ and HF is calculated to be highly exothermic, i.e., by 73.9 kcal $mol^{-1}$. Despite this strong thermodynamic driving force for decomposition, **1** is stable at moderate temperatures.[4] This relatively high kinetic stability is consistent with the fact that all the unimolecular decomposition pathways that we have considered have energy barriers which are higher than 38 kcal $mol^{-1}$. The lowest activation energy for the decomposition of **1** of 38.8 kcal $mol^{-1}$ is found for the unimolecular decomposition of $CH_3OF$ *via* **TS 1**, according to mechanism *a* in Scheme 1. The rate-determining step along path *b* of Scheme 1 arising from the first step, the O−F bond dissociation, has a higher calculated activation barrier of 45.9 kcal $mol^{-1}$ (G2).[33] This dissociation energy is 2.1 kcal $mol^{-1}$ lower than in HOF (44.2 kcal $mol^{-1}$ as compared to 46.3 kcal $mol^{-1}$ in $CH_3OF$, both at G1),[34] reflecting the stabilizing effect of the methyl group in $CH_3O^\bullet$ relative to $HO^\bullet$.

The rate-determining step along path *c* in Scheme 1, the synchronous O−F bond dissociation−1,2 H migration *via* **TS 3**, is calculated to lie 48.1 kcal $mol^{-1}$ above the reactants. All subsequent steps have lower TSs; the next highest is the

(27) The attack of $F^\bullet$ on $H_3CO^\bullet$ (and $H_2COH^\bullet$) most probably leads initially to a complex between the radicals. We could not locate these structures because the HF and the MP2 methods, used in this study, are not suitable for the optimization of complexes between two radicals. However, we believe that the presence of such weakly-bonded complexes will not significantly affect the rate-determining steps of the decomposition of $CH_3OF$.

(28) Pople, J. A.; Frisch, M. J.; Luke, B. T.; Blinkley, J. S. *Int. J. Quantum Chem., Quantum Chem. Symp.* **1983**, *17*, 307.

(29) (a) Pau, C. F.; Hehre, W. J. *J. Phys. Chem.* **1982**, *86*, 1252. (b) Schlegel, H. B.; Robb, M. A. *Chem. Phys. Lett.* **1982**, *93*, 43.

(30) (a) Suenra, R. D.; Lovas, F. J.; Pickett, H. M. *J. Mol. Spectrosc.* **1986**, *119*, 446. (b) Schaefer, L.; von Alseney, C.; Williams, J. O.; Scardale, J. N.; Geise, H. J. *J. Mol. Struct.* **1981**, *76*, 349.

(31) Yamashita, K.; Yaaba, T.; Fukui, K. *Theor. Chim. Acta* **1982**, *60*, 523.

(32) For the similar HF elimination from $CF_3OH$ see: Francisco, J. S. *Chem. Phys.* **1991**, *150*, 19.

(33) The alternative mechanism in which $H_3CO^\bullet$ eliminates unimolecularly a hydrogen radical to produce $H_2C{=}O$ is higher in energy by 17.8 kcal $mol^{-1}$ (at CASSCF/[4s3p2d1f/3s2p1d]) and also involves a barrier of 23.4 kcal $mol^{-1}$. See: Walch, S. P. *J. Chem. Phys.* **1993**, *98*, 3076. This mechanism therefore cannot compete with the path *via* **TS 2**.

(34) Pople, J. A.; Curtiss, L. A. *J. Chem. Phys.* **1989**, *90*, 2833.

**Table 3.** MP4/6-311+G**, G1, and G2 Calculated Absolute Energies (hartrees) and Relative Energies, $\Delta E$, of the Investigated Species

| | MP4/6-311+G** [a] | $\Delta E$ (kcal/mol) | G1 (au) | $\Delta E$ (kcal/mol) | G2 (au) | $\Delta E$ (kcal/mol) | freq ($cm^{-1}$) |
|---|---|---|---|---|---|---|---|
| $CH_3OF$(**1a**) | −214.43959 | 0 | −214.56856 | 0 | −214.57117 | 0 | |
| $CH_2O$ (**2**) + HF (**3**) | −214.55509 | −72.5 | −214.68437 | −72.6 | −214.68889 | −73.9 | |
| $CH_3O^•$ (**4**) + $F^•$ (**5**) | −214.37433 | +40.9 | −214.49470 | +46.3 | −214.49791 | +45.9 | |
| **TS 1** | −214.37961 | +37.6 | −214.50536 | +39.7 | −214.50925 | +38.8 | −2585.1 |
| **TS 2** | −214.40229 | +23.4 | −214.53271 | +22.5 | −214.53674 | +21.6 | −2600.9 |
| **TS 3** | −214.36301 | +48.1 | −214.49108 | +48.6 | −214.49449 | +48.1 | −1845.2 |
| **TS 4** | −214.46706 | −17.3, −49.5[b] | −214.61539 | −67.4[b] | −214.62037 | −66.9[b] | −43.2 |
| **TS 5** + HF (**3**) | −214.41858 | +32.6,[d] 85.7[e] | −214.55137 | +45.4,[d] 83.5[e] | −214.55611 | +45.6,[d] 83.3[e] | −2168.6 |
| **TS 6** | −214.49249 | +33.2 | −214.49066 | +48.9 | −214.49473 | +47.9 | −1895.5 |
| **TS 7** | −214.49079 | +50.4 | −214.62391 | +54.2[c] | −214.62785 | +54.4[c] | −1808.8 |
| CHOH (**7**) + HF (**3**) | −214.47058 | −19.4 | −214.62372 | −38.1 | −214.62878 | −37.7 | |
| $CH_2OH^•$ (**6**) + $F^•$ (**5**) | −214.38815 | +32.3 | −214.50794 | +38.5 | −214.51370 | +36.1 | |
| $CH_2FOH$ (**8**) | −214.57057 | −82.6, −9.7[e] | −214.71026 | −88.9, −16.2[e] | −214.71449 | −89.9, −16.1[e] | |

[a] At the MP2(fu)/6-31G* geometry. [b] Relative to $CH_2OH^•$ (**6**) + $F^•$ (**5**). [c] Relative to $FCH_2OH$ (**8**). [d] Relative to CHOH (**7**) + HF (**3**). [e] Relative to $CH_2O$ (**2**) + HF (**3**).

**Chart 1.** Relative Energies at G2 for the Unimolecular Decomposition Pathways *a*−*d* of Scheme 1

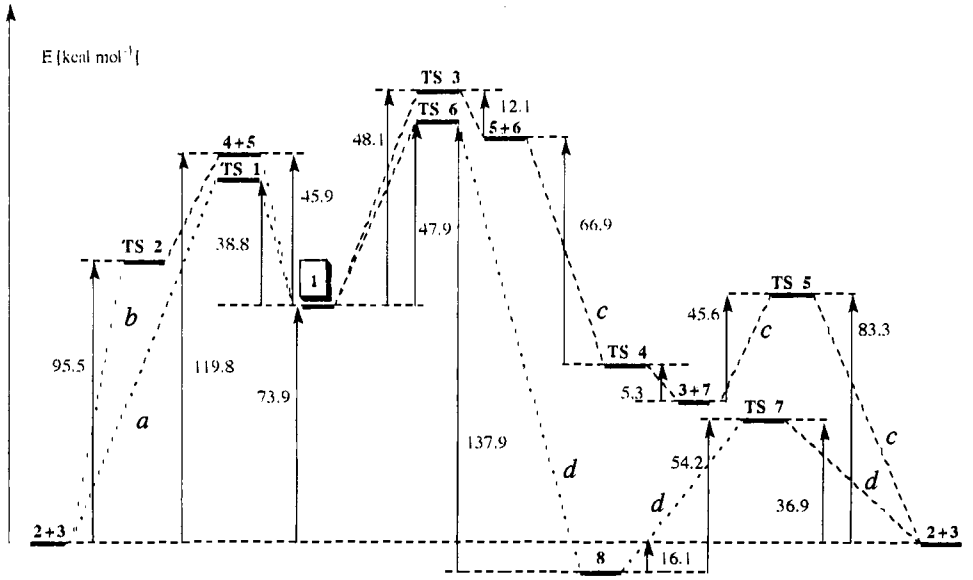


**Table 4.** Absolute and Relative Entropies, $\Delta S$, and Free Energies $\Delta G$ at MP2(fu)/6-31G* for Species of Interest

| | $S$ (eu) | $\Delta S$ (eu) | $T\Delta S$(300 K) (kcal/mol) | $T\Delta S$(230 K) (kcal/mol) | $\Delta G$(300 K) (kcal/mol) | $\Delta G$(230 K) (kcal/mol) |
|---|---|---|---|---|---|---|
| $CH_3OF$ (**1a**) | 62.2 | | | | | |
| $CH_3O^•$ + $F^•$ | 94.9 | 32.7 | 9.8 | 7.5 | 36.1 | 38.4 |
| **TS 1** | 61.5 | −0.7 | −0.2 | −0.2 | 39.0 | 39.0 |
| **TS 3** | 61.7 | −0.5 | −0.2 | −0.1 | 48.3 | 48.2 |
| **TS 6** | 61.5 | −0.7 | −0.2 | −0.2 | 48.1 | 48.1 |

isomerization of *trans*-CHOH carbene (**7**) to $CH_2O$ (**2**), having a barrier of 45.6 kcal $mol^{-1}$.

The first step along path *d* in Scheme 1 *via* **TS 6** has a calculated barrier of 47.9 kcal $mol^{-1}$, leading to $H_2FCOH$ (**8**), which is the global minimum on the $CH_3OF$ surface lying 90.0 kcal $mol^{-1}$ below **1**. The subsequent HF elimination from **8** *via* **TS 7**[31] to give the final products is the rate-determining step along this reaction path having a barrier of 54.2 kcal $mol^{-1}$.

Path *a* in Scheme 1 is clearly the lowest *enthalpy* reaction path for the decomposition of **1**. However, in order to establish computationally the most favorable unimolecular mechanism followed experimentally in the gas phase, the Gibbs free energies of all the above-mentioned mechanisms should be computed. The calculated entropies for the species of interest are presented in Table 4. As expected, the entropy change is significant only for the dissociative pathway *b* ($T\Delta S$ = 9.8 kcal $mol^{-1}$ at 300 K), whereas it is very small for the cyclic unimolecular transition states along mechanisms *a*, *c*, and *d* in Scheme 1.[35] As a result for the multistep mechanisms, $\Delta G^‡$ and $\Delta H^‡$ are nearly the same, while for the dissociative mechanism *b* $\Delta G^‡$ is lower than $\Delta H^‡$ by 9.8 kcal $mol^{-1}$ at room temperature. Thus, for the dissociative mechanism *b*, the calculated $\Delta G^‡$ is 38.4 kcal $mol^{-1}$ at 300 K and 36.1 kcal $mol^{-1}$ at 230 K. *Thus, as a result of the effect of entropy mechanisms a and b of Scheme 1 are predicted to have very similar activation free energies.* The activation energies for the rate-determining steps along the multistep mechanisms *c* and *d* of 47.9 and 54.2 kcal $mol^{-1}$, respectively, are significantly higher. It can be concluded that neither path *c* nor path *d* in Scheme 1 is the favored mechanism for the unimolecular decomposition of $CH_3OF$.

*The calculated activation free energies for mechanisms a and b in Scheme 1 are so close, especially at room temperature, that we have to conclude that in the gas phase under very high pressure conditions (or in solution) both pathways are likely mechanisms for the thermal unimolecular decomposition of $CH_3OF$ to $CH_2O$ and HF and they may actually compete.* However, mechanism *b* may not compete effectively under low pressure conditions because of the low probability of reaching **TS 2** after **1** has fragmented to give the $CH_3O^•$ and $F^•$ radicals. We show

(35) The change of the reaction entropy in the second step of path *b via* **TS 2** is not large enough to change the rate-determining step, which also on the $\Delta G^‡$ surface remains to be the dissociation of $CH_3OF$ to **4** + **5**. $\Delta G^‡$ for the formation of **4** + **5** is more than 16 kcal $mol^{-1}$ higher than for **TS 2**.

**Table 5.** Calculated Kinetic Isotope Effects for the Decomposition of **1a** *via* **TS 1** (Path *a* in Scheme 1) and Dissociation to $CH_3O^{\bullet}$ + $F^{\bullet}$ (Path *b* in Scheme 1)

| isotopic label[a] | $k_H/k_D$ (298 K) | | $^{12}C/^{13}C$ (298 K) | |
|---|---|---|---|---|
| | path *a* | path *b* | path *a* | path *b* |
| 1-$^2$H | 4.04 | 1.13 | 1.02 | 1.01 |
| 2-$^2$H | 1.10 | 1.13 | | |
| 3-$^2$H | 1.10 | 1.21 | | |
| 1,2,3-$^2$H | 5.11 | 1.52 | | |

[a] For atom labeling see **TS 1** in Scheme 1.

below that isotope effects can be used to establish experimentally which is the actual unimolecular decomposition mechanism of $H_3COF$.

**5. Kinetic Isotope Effects.** Kinetic isotope effects can be calculated by solving the Bigeleisen equation[36] using Cartesian force constants from *ab initio* calculations. This equation gives ratios of rates for a particular process for the unsubstituted and isotopically substituted species ($k_H/k_D$ in this case). In the absence of symmetry number effects the deviation from unity of an isotope effect on an equilibrium constant (in our case between the reactants (AX; X = H, D) and the products or transition states (BX; X = H, D) is given by eq 2, where $u_i = h\nu_i/kT$.

$$\frac{k_H}{k_D} = \prod_{i=1}^{3N-6} \frac{u_i(BH)}{u_i(BD)} \frac{1 - e^{-u_i(BD)}}{1 - e^{-u_i(BH)}} \frac{e^{u_i(BD)/2}}{e^{u_i(BH)/2}} \times \prod_{i=1}^{3N-6} \frac{u_i(AD)}{u_i(AH)} \frac{1 - e^{-u_i(AH)}}{1 - e^{-u_i(AD)}} \frac{e^{u_i(AH)/2}}{e^{u_i(AD)/2}} \quad (2)$$

We used the program QUIVER[13] to calculate the isotope effects for the two crucial steps in mechanisms *a* and *b* of Scheme 1, i.e., **1a** → **TS 1** (mechanism *a*) and **1a** → **4** + **5** (mechanism *b*). The frequencies were derived from the appropriate isotopic masses together with the force constants which were calculated at MP2(fu)/6-31G*. Isotope effects arising from single isotopic label ($^2$H, $^{13}$C) as well as for the trideuterated species were calculated at 298 K. The derived data are summarized in Table 5.

As expected qualitatively the primary isotope effect for **1a** → **TS 1** along mechanism *a* is significantly larger than the secondary isotope effect for **1a** → **4** + **5** in mechanism *b*. The $^{13}$C isotope effects in both mechanisms are as expected very small (1.01 and 1.02). For the O−F bond dissociation step, **1a** → **4** + **5** (mechanism *b*) the substitution of all three hydrogens by deuteriums leads to a calculated $k_H/k_D$ ratio of 1.52. For the **1a** → **TS 1** step (mechanism *a*) the dissociating hydrogen, $H^1$, in **TS 1** shows a very large isotope effect of 4.04. The effect of the other hydrogens, $H^2$ and $H^3$, is small (1.10), and the trideuterated $D_3COF$ is calculated to have a very large isotope effect of 5.11 compared to only 1.52 in mechanism *b*. The much larger calculated isotope effect for the decomposition of $CD_3OF$ along mechanism *a* than for mechanism *b* suggests that experimental studies comparing the rates of decomposition of $H_3COF$ and $D_3COF$ (or examination of the products for the decomposition of $DH_2COF$) should be able to differentiate between these competing pathways.[38]

## Conclusions

High level *ab initio* calculations which include electron correlation can reproduce the IR and NMR spectra of $CH_3OF$. Calculations of several possible decomposition pathways of $CH_3OF$ to $CH_2O$ and HF lead to two competing pathways as the most likely mechanisms: the first involving 1,2-HF elimination and the second O−F bond dissociation as the rate-determining steps. Both processes have similar activation free energies. The calculated kinetic isotope effects for these two mechanisms are very different, suggesting it as an experimental criterion to evaluate the favored decomposition mechanism of **1**. We hope that our study will prompt such experimental studies. We are currently studying the acetonitrile−$CH_3OF$ complex[5a,37] in order to understand how coordination with acetonitrile stabilizes $CH_3OF$. We are also studying higher homologs of alkyl hypofluorites such as EtOF, *i*-PrOF, and *t*-BuOF in order to evaluate computationally their properties, in particular their thermodynamic and kinetic stabilities.

**Acknowledgment.** We thank Professor Martin Saunders for supplying us with a copy of the QUIVER program and Professor Shlomo Rozen for discussions. The research was supported by the Fund for the Promotion of Research at the Technion. K.A. thanks the Minerva-Foundation for a postdoctoral scholarship.

JA951069N

(36) For reviews see: (a) Melander, L.; Saunders, W. H., Jr. *Reaction Rates of Isotopic Molecules*; Wiley: New York, 1980. (b) Collins, C. J., Bowan, N. S., Eds. *Isotope Effects in Chemical Reactions*, ACS Monograph No. 167; Van Nostrand Reinhold: New York, 1970.

(37) (a) Rozen, S.; Bareket, Y.; Kol, M. *Tetrahedron* **1993**, *49*, 8169. (b) Dunkelberg, O.; Haas, A.; Klapdor, M. F.; Mootz, D.; Poll, W.; Appelmann, E. H. *Chem. Ber.* **1994**, *127*, 1871.

(38) **Note Added in Proof.** Most recently, S. Rosen et al. have succeeded in isolating $CD_3CD_2OF$ and $CD_3CH_2OF$, but attempts to isolate $CH_3CH_2OF$ have failed. These findings are consistent with a high kinetic isotope effect and thus with the operation of mechanism *a* (we thank Professor Rosen for making this information available to us prior to publication).